

# Synthesis of Gold Nano- and Microplates in Hexagonal Liquid Crystals

Luyan Wang,<sup>†</sup> Xiao Chen,<sup>\*,†</sup> Jie Zhan,<sup>‡</sup> Yongcun Chai,<sup>†</sup> Chunjie Yang,<sup>†</sup> Limei Xu,<sup>†</sup> Wenchang Zhuang,<sup>†</sup> and Bo Jing<sup>†</sup>

Key Laboratory of Colloid and Interface Chemistry, Shandong University, Ministry of Education, Jinan 250100, China, and Institute of Crystal Material, Shandong University, Jinan 250100, China

Received: November 6, 2004; In Final Form: December 21, 2004

Single-crystalline gold nano- and microplates with triangular or hexagonal shapes are synthesized by reduction of HAuCl<sub>4</sub> in lyotropic liquid crystal (LLC) mainly made of poly(ethylene oxide)–poly(propylene oxide)–poly(ethylene oxide) block copolymers and water after adding a small amount of capping agents, cetyltrimethylammonium bromide (CTAB) or tetrabutylammonium bromide (TBAB). During the growth of such plates, capping agents play the crucial role. It is found that there is an optimal value of CTAB or TBAB concentration for producing microplates. The selective adsorption of CTAB or TBAB on certain crystallographic facets may be the key point of the supposed mechanism. Although LLC does not really act as a template, it provides an ordered structure confining CTAB as well as the nascent metal nuclei, which enhances the oriented attachment of nuclei and thus the consequent growth of single-crystal plates.

## 1. Introduction

Inorganic nanocrystals have been widely studied in the past decades because of their great potential applications in electronics, biology, photonics, and so forth.<sup>1</sup> Although the synthesis of spherical nanocrystals is well developed for many kinds of materials, fabrication of an anisotropic nanocrystal is still a challenge for researchers in this field. The shape and size are key parameters in such preparation because of their close relation to the physical and chemical properties of final material.<sup>2</sup> Many efforts have been devoted to prepare such anisotropic inorganic nanocrystals such as rods, wires, cubes, disks, and other special morphologies.<sup>3</sup> Particularly, one- or two-dimensional (1D or 2D) nanostructures for noble metals attract much attention.<sup>4</sup> Nanorods or wires of silver and gold, with controllable diameters and aspect ratios, have been synthesized by electrochemical, photochemical, templating, and seeding growth methods.<sup>5–13</sup> 2D silver nanodisks are also intensely investigated by various solution-phase methods.<sup>14–16</sup> However, in contrast to a large amount of reports on gold nanorod and silver nanodisks, few concern systems of gold nanodisks or planar nanoparticles though triangular gold nanoplates had been observed more than 50 years ago.<sup>17</sup> The methods having been used are generally by reduction of Au<sup>III</sup> to Au<sup>0</sup> through chemical, photochemical, or biological process.<sup>18–23</sup> For example, a chemical synthetic method within inverse micelles was used by Stoeva et al. to get platelike gold superlattices from nanoparticles assembling.<sup>18</sup> Liz-Marzan's group obtained flat triangular and hexagonal nanoplates of ~50–200 nm in diameter, by reduction of Au<sup>III</sup> with salicylic acid in aqueous solution, accompanied with smaller close-to-spherical gold nanoparticles.<sup>19</sup> The produced polygons are of relatively low concentration, which leads to only the longitudinal resonance visible in UV–vis spectrum. Photoreduction process was employed by Zhou et al. and Ibano et al. to produce triangular or hexagonal gold nanoplates.<sup>20,21</sup>

The capping agents in the reaction systems, poly(vinyl alcohol) and dimyristoyl-L- $\alpha$ -phosphatidyl-DL-glycerol, are considered to play important roles in controlling the nanoparticle shape while their growth mechanisms have not been discussed in detail. In addition, Tsuji et al. reported a microwave–polyol method to produce gold nanoplates but with an unsatisfactory shape control since the product was a mixture of nanoplates and square or spherical particles.<sup>22</sup>

Though these different ways have been established to get anisotropic gold nanoplates, results are not promising because these methods are often characterized by relative low yields or small product sizes. Shape control of metal nanoparticles has proved more difficult, and there is still great interest in developing new methods for systematic manipulation of platelike gold nanocrystals and investigating their growth mechanism. A biological method is recently reported to obtain high-yield gold nanoprisms with the extract from the lemongrass plant as the reducer.<sup>23a</sup> Gold microplates are obtained from a thermal process at 70 °C as well as from a wet-chemical route in an aqueous medium.<sup>23b,23c</sup> We have also tried the preparation of gold nano- and microplates from lyotropic liquid crystals (LLC) made of poly(ethylene oxide)–block–poly(propylene oxide)–block–poly(ethylene oxide) (PEO–PPO–PEO) block copolymers.<sup>24</sup> In this paper, we extend this research trying to obtain products of controllable shape and size. More attention is paid to different factors affecting on product formation and growth mechanism. Cetyltrimethylammonium bromide (CTAB) and tetrabutylammonium bromide (TBAB), as capping agents, are added to systematically control the morphology of gold products.

## 2. Experimental Section

**Materials.** The amphiphilic block copolymer Pluronic P123 (EO<sub>20</sub>PO<sub>70</sub>EO<sub>20</sub>, Mn = 5800) is purchased from Aldrich. Hydrogen tetrachloroauric acid (HAuCl<sub>4</sub>·4H<sub>2</sub>O, ≥99.9%), CTAB (99.0%), and TBAB (≥99.0%) are all purchased from Shanghai Reagent Co. The water used is highly purified with the resistivity ≥18.0 M $\Omega$ ·cm. All chemicals are used as received without further purification.

\* To whom correspondence may be addressed. E-mail: xchen@sdu.edu.cn. Tel: +86-531-8365420. Fax: +86-531-8564750.

<sup>†</sup> Key Laboratory of Colloid and Interface Chemistry.

<sup>‡</sup> Institute of Crystal Material.

**Synthesis of Gold Products.** On the basis of the phase diagram<sup>25</sup> reported by Alexandridis, Pluronic P123 can form a hexagonal phase at higher concentration (weight percentage of 40–50%) when mixed with water at room temperature. In our study, 45% P123 is selected where the PEO–PPO–PEO molecules self-assemble into cylinders with PEO blocks in water domains. To prepare gold nanocrystals, tetrachloroauric acid aqueous solution (0.03 or 0.015 M) instead of water is used to construct hexagonal phase with PEO–PPO–PEO and CTAB or TBAB of lower weight percentages. The samples are sealed in glass tubes and left at room temperature for further study.

**Small-Angle X-ray Scattering (SAXS) Measurement.** Phase behaviors of LLCs are investigated by SAXS on a HMBG-SAX X-ray small angle system (Austria) with Ni-filtered Cu K $\alpha$  radiation (0.154 nm) operating at 50 kV and 40 mA. The sample-to-detector distance is 277 cm. The temperature is kept at  $25 \pm 0.1$  °C. The relative positions of SAXS scattering peaks along the scattering vector ( $q$ ) axis are used to determine the lyotropic phase structure. For hexagonal structure (cylindrical assemblies crystallized in a hexagonal lattice), the peak positions should obey the relation  $1:\sqrt{3}:2:\sqrt{7}$ .<sup>25</sup>

**Characterization of Products.** Morphologies of gold particles are observed under a JEM-100CX II (JEOL) transmission electron microscope operated at 100 kV. To prepare transmission electron microscopy (TEM) samples, the reacted mixtures are dispersed in water under sonication and centrifuged at  $\sim 3600$  rpm for 10 min. Then the upper solution containing unreduced ions and unbound surfactant molecules is removed. Such obtained samples are redispersed in water. A little drop of resulting dispersion is put onto a Formvar-covered copper grid (230 mesh) for TEM measurement. The optical properties of obtained gold products dispersed in water are characterized on a HP 8453E UV–vis spectrometer with resolution of 1 nm.

### 3. Results and Discussion

**3.1. Preparation of Gold Products from CTAB-Doped Systems. 3.1.1. LLC Phase Structures.** The SAXS patterns of P123 samples are shown in Figure 1. The relative position of SAXS diffraction peaks along the scattering vector ( $q$ ) axis is used to determine the LLC phase structure. The lattice spacing ( $d$ ) is the distance between adjacent rows of cylinders in the hexagonal structure and is determined from the first peak position ( $q_1$ ).<sup>25</sup> All systems here maintain structural characteristics of the hexagonal phase with their  $d$  spacings being listed in Table 1. It can be noted that all systems accommodating gold products exhibit enlarged  $d$  values, which is easy to understand when considering the swelling effect of particles formed in LLC phase. From Figure 1, we can also find differences between curve shapes for samples with or without gold formation (parts a–c of Figure 1). First, the intensity of peaks 1 and 2 become drastically weaker for systems having Au<sup>III</sup> reduction, which may originate from the deterioration of long-range ordering in the LLC phase by included gold particles and decreased viscosity due to oxidation of ethylene oxide chains in polymer molecules. Another change is the elevation of scattering curve in the low  $q$  region for samples a<sub>1</sub>, b<sub>1</sub>, and c<sub>1</sub>, which is an obvious indication for the production of gold nanoparticles according to the analysis by Firestone.<sup>26</sup> For systems with  $\sim 1.5$ – $2.0\%$  CTAB, however, two SAXS patterns before and after reduction are similar to each other, suggesting that products do not much influence the structures of reacting systems, consistent with the TEM observation as discussed in the following section.

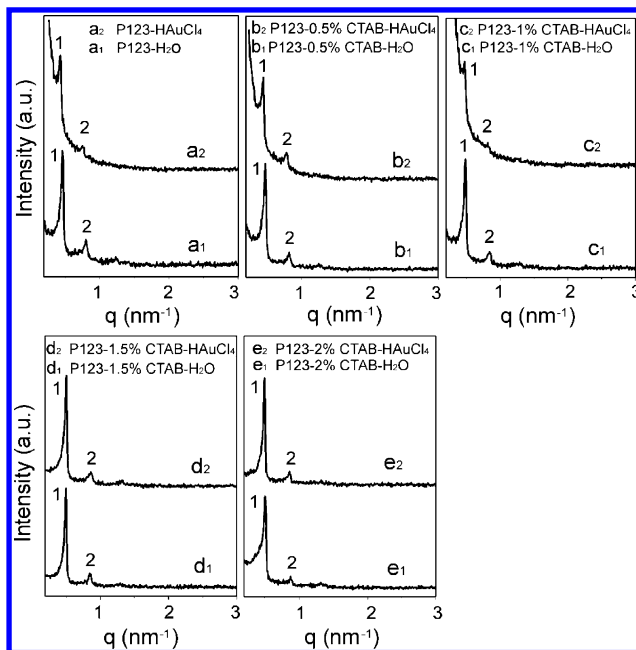


**Figure 1.** SAXS patterns of P123 (45%) hexagonal liquid crystal phases measured 3 days after preparation. HAuCl<sub>4</sub> concentration is 0.03 M.

**TABLE 1: Lattice Spacings ( $d$ ) for LLC Phases with Different Compositions**

systems <sup>a</sup>	$d$ (nm)	systems <sup>a</sup>	$d$ (nm)
a <sub>1</sub>	13.6	a <sub>2</sub>	14.1
b <sub>1</sub>	13.2	b <sub>2</sub>	13.7
c <sub>1</sub>	12.8	c <sub>2</sub>	13.3
d <sub>1</sub>	12.6	d <sub>2</sub>	12.8
e <sub>1</sub>	12.4	e <sub>2</sub>	12.6

<sup>a</sup> System composition corresponds to those denoted in Figure 1.

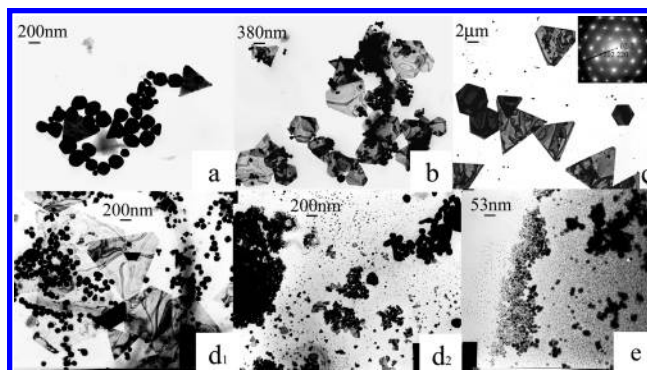


**Figure 2.** TEM images of gold nano- and microcrystals obtained from P123–HAuCl<sub>4</sub> (0.03 M) systems measured 3 days after preparation. CTAB concentrations are (a) 0%, (b) 0.5%, (c) 1.0%, (d) 1.5%, and (e) 2.0%.

**3.1.2. Structural Characterization of Gold Products.** In ordered cylindrical arrays self-assembled from PEO–PPO–PEO, the reduction occurs in the aqueous domain and PEO blocks will slowly reduce Au<sup>III</sup> ions to Au through oxidation of their oxyethylene groups.<sup>27</sup> TEM images for samples produced from different systems are shown in Figure 2. Spherical nanoparticles are main products (ca. 200 nm) coexisting with few triangular nanoplates when no CTAB is added. Upon an increase of the CTAB concentration to 0.5%, more platelike gold nanocrystals appear accompanied with spheres (Figure 2b). As shown in Figure 2c, however, adding 1.0% CTAB into the LLC results in much more and larger gold plates. They exhibit equilateral or truncated triangular and hexagonal

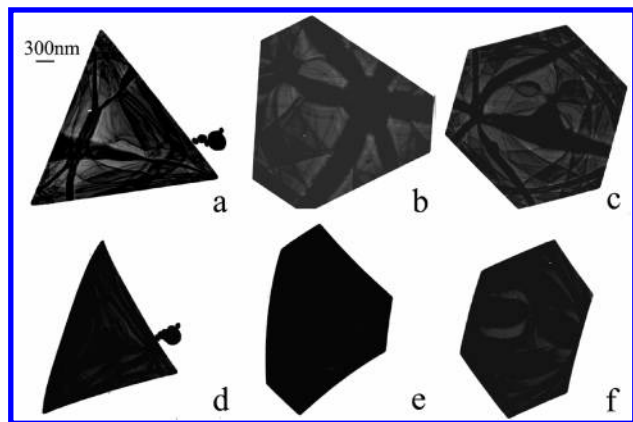


**Figure 3.** TEM images of nanocrystals prepared from P123–CTAB (1.0%)–HAuCl<sub>4</sub> (0.03 M) system. a, b, and c represent an equilateral triangle, a truncated triangle, and a hexagon, respectively. d, e, and f represent their corresponding images from tilt experiments with the tilt angle of  $-50^\circ$ .

shapes with the edge size even longer than  $10\ \mu\text{m}$ . The triangles and hexagons are characterized by a low and uniform contrast, indicating a flat feature. When CTAB concentration rises to 1.5%, the product morphology changes greatly. It exhibits both diversity and decreased size verified also by SAXS patterns (parts d and e of Figure 1), including nanoplates, particles aggregates, or monodispersive nanoparticles (with diameters even smaller than 1 nm, shown in Figure 2d). A similar result occurs in a system with 2.0% CTAB, except for the smaller particles and less nanoplates.

To investigate the nature of obtained microplates, tilt experiments are performed, respectively. The electron diffraction (ED) pattern (inset in Figure 2c) clearly suggests a face-centered cubic (fcc) single crystal with an atomically flat surface and its  $[-111]$  orientation parallel to the electron beam. All facets of single crystals parallel to the grid are preferentially along  $\{111\}$  planes. Such features indicate the faceted morphology of gold microplates and their inherent anisotropy, which is important since many optical and electronic properties will depend on the orientation of crystal materials.<sup>18</sup>

The flatness of these plates is reflected by their low contrast appearance. They are proved also not pyramids by TEM observation under tilt angle. It is found that the projection shapes of triangular and hexagonal particles are similar to original samples and also in uniform contrast (see Figure 3), indicating the plate but not pyramid nature.<sup>28</sup>

**3.1.3. Optical Properties.** Optical properties of prepared gold nano- and microcrystals are strongly related to their shape and size, which seem to be tailored by CTAB molecules as seen in

TEM results. To further study such manipulation effect and monitor the products formation, the optical absorption properties of obtained product dispersions are compared as a function of CTAB concentration. As shown in Figure 4A, the UV–vis absorption curves for five investigated samples change gradually with varying CTAB amount. On the basis of the shape of the curves a<sub>1</sub>, b<sub>1</sub>, and c<sub>1</sub>, we can conclude that the main products of these three systems are spherical nanoparticles at beginning of reduction. The symmetrical shape of absorption peak in curves a<sub>1</sub> and b<sub>1</sub> reflects a uniform size distribution of spherical particles. With an increase in CTAB concentration to 1.0%, a new shoulder band at  $\sim 660\text{--}740\ \text{nm}$  appears on the spectrum except for the original absorption peak centered around 560 nm (Figure 4c<sub>1</sub>), which may be attributed to the occurrence of platelike particles and product aggregation.<sup>29</sup> For samples with 1.5 and 2.0% CTAB, there is no distinct absorption exhibiting slower reduction rate of Au<sup>III</sup> possibly due to the capping effect of CTAB molecules.

With extended reaction time, spectral changes of the above systems are depicted in Figure 4B. The surface plasmon resonance (SPR) band at 547 nm (Figure 4a<sub>1</sub>) is now red-shifted to 563 nm for a system without CTAB (Figure 4a<sub>2</sub>), and its shape becomes also unsymmetrical, reflecting the formation of larger particles and their aggregates mixing with few platelike structures (Figure 2a). For a sample with 0.5% CTAB, the red-shifted band becomes broader owing to nanoplate formation (Figure 4b<sub>2</sub>). At 1.0% CTAB, two peaks begin to occur, including a broad peak at 600–800 nm relating to the large-scale formation of platelike products and the band around 569 nm (Figure 4c<sub>2</sub>). Note that systems with more CTAB exhibit still a broad and flat feature extending well into the red (curves d<sub>2</sub> and e<sub>2</sub> of Figure 4), which is similar to those of other nanostructured gold materials, such as thin films and nanoparticle aggregates.<sup>29</sup> On the basis of TEM images in parts d and e of Figure 2, it is reasonably considered that such changes are originated from the aggregation and strong interaction of gold products.<sup>19,29,30</sup>

**3.2. Effect of TBAB.** To compare the capping effect, TBAB is used instead of CTAB with a weight percentage of 0.5–2.0%. Like CTAB, TBAB affects little on the hexagonal phase without HAuCl<sub>4</sub> and the phase repeat spacings are nearly the same as those without TBAB. When HAuCl<sub>4</sub> is introduced as the precursor, the SAXS curves (not shown here) after reduction exhibit features just like those in Figure 1, showing deterioration of the hexagonal phase because of products formation and oxidation of ethyleneoxide groups.

TEM images of products from these samples are shown in Figure 5. Although both samples with less TBAB (0.5 and 1.0%)

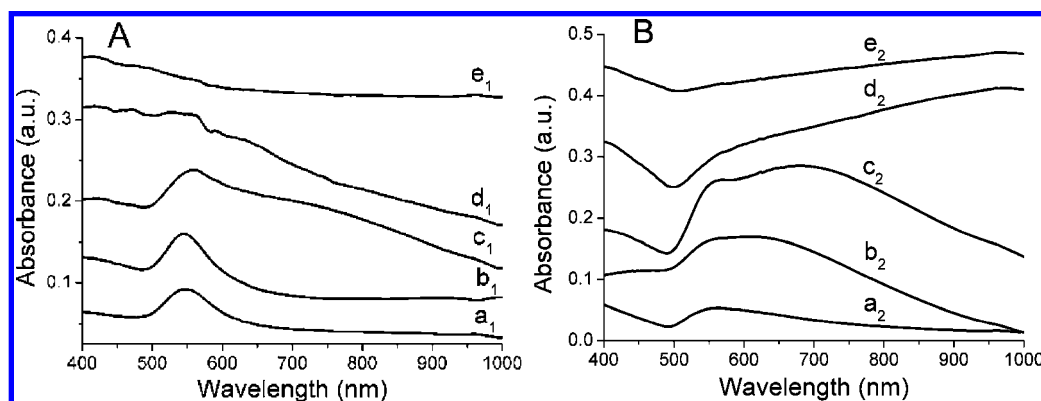


**Figure 4.** UV–vis absorption spectra of gold products prepared, respectively, from P123–HAuCl<sub>4</sub> (0.03 M) systems with CTAB concentration at (a) 0%, (b) 0.5%, (c) 1.0%, (d) 1.5%, and (e) 2.0%. They are measured, respectively, at 5 h (A) and 3 days (B) after sample preparation.

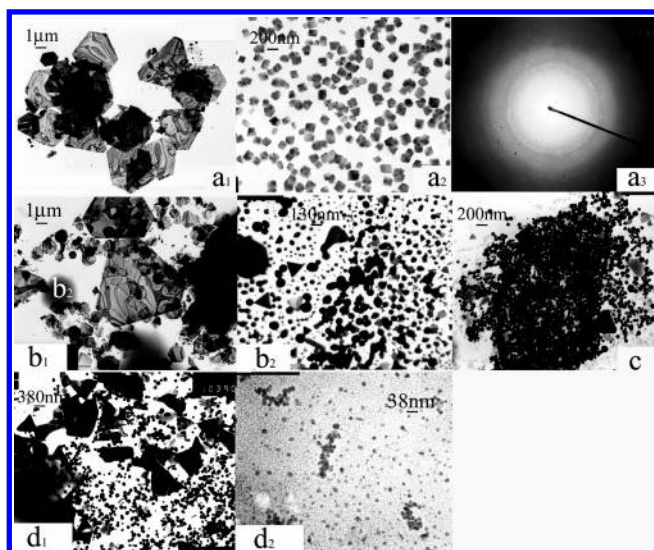


**Figure 5.** TEM images of gold products formed in P123-HAuCl<sub>4</sub> (0.03 M) systems measured 3 days after preparation with adding TBAB (a) 0.5%, (b) 1.0%, (c) 1.5%, and (d) 2.0%.

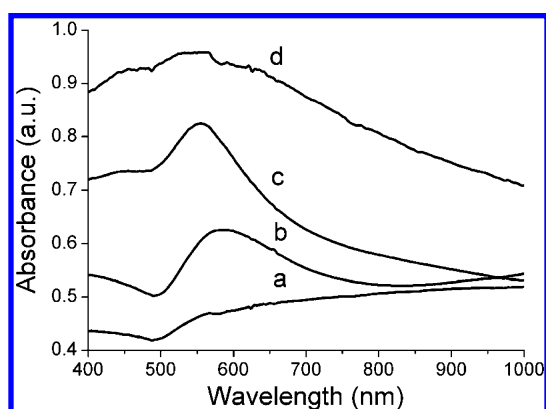


**Figure 6.** UV-vis absorption spectra of gold products prepared, respectively, from P123-HAuCl<sub>4</sub> (0.03 M) systems with TBAB concentration at (a) 0.5%, (b) 1.0%, (c) 1.5%, and (d) 2.0% measured 3 days after sample preparation.

exhibit particles of platelike shape (curves a<sub>1</sub> and b<sub>1</sub> of Figure 5), products with other morphologies are also formed. In a 0.5% TBAB sample, platelets with quadrangular shape are observed (Figure 5a<sub>2</sub>) in a large amount besides gold plates, as indicated by their optical absorption shape (Figure 6a). It keeps increasing into the IR region with no indication of leveling off, which may result from the strong interaction between small particles growth and aggregation of quadrangular or platelike particles.<sup>29,30</sup> The ED pattern (Figure 5a<sub>3</sub>) shows their polycrystalline feature. In a 1.0% TBAB system, such platelets also appear but in a lesser amount. It should be noted that another type of product emerges when we enlarge the area marked b<sub>2</sub> in Figure 5b<sub>1</sub>, i.e., smaller particles and their aggregates with varied shapes (see Figure 5b<sub>2</sub>). The absorption curve b in Figure 6, showing a broad peak around 560 nm with a running-up tail after 850 nm, should be attributed to mixing and aggregation of plates and particles and to the interactions between them.<sup>19,23,29,30</sup> When TBAB concentration is increased to 1.5 and 2.0%, the product size is reduced obviously. Figure 5c presents mainly spherical nanoparticles with relatively uniform size corresponding to typical SPR adsorption feature (Figure 6c). In curves d<sub>1</sub> and d<sub>2</sub> of Figure 5 (2.0% TBAB), more spherical nanoparticles appear with a large size range varying from 1 to 200 nm, accompanied with few irregular plates, corresponding to a broad shape of the UV-vis absorption curve (Figure 6d).<sup>31</sup> These results suggest that,

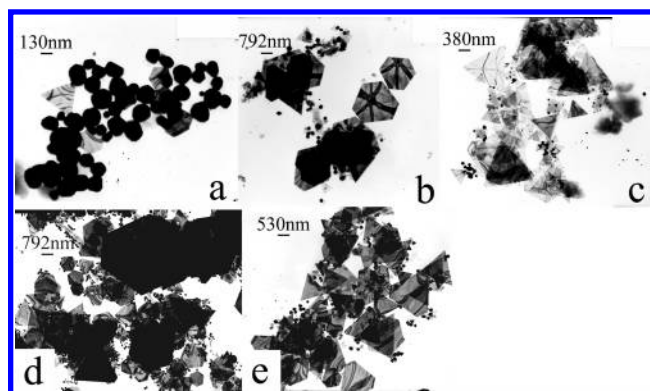


**Figure 7.** TEM images of gold products formed in P123-HAuCl<sub>4</sub> (0.015 M) systems with adding (a) 0%, (b) CTAB 0.5%, (c) CTAB 1.0%, (d) TBAB 0.5%, and (e) TBAB 1.0% measured 3 days after preparation.

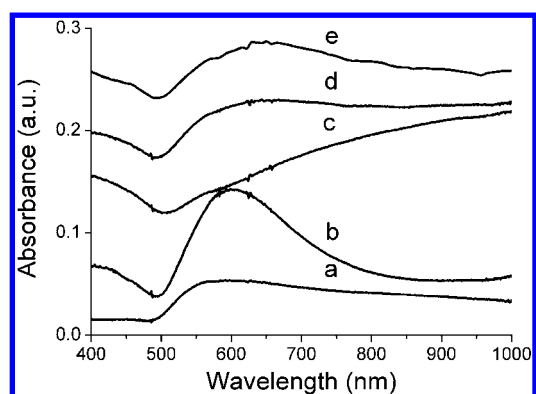


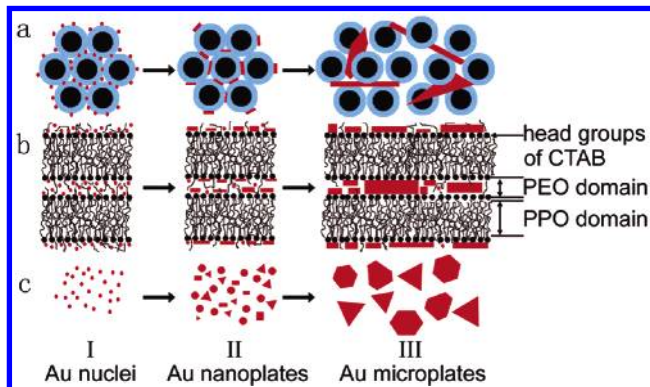
**Figure 8.** UV-vis absorption spectra of gold products prepared, respectively, from P123-HAuCl<sub>4</sub> (0.015 M) systems with CTAB or TBAB concentration at (a) 0%, (b) CTAB 0.5%, (c) CTAB 1.0%, (d) TBAB 0.5%, and (e) TBAB 1.0% measured 3 days after sample preparation.

when short-chain branched TBAB is added to reaction systems, products tend to exhibit diversity of morphologies, with a mechanism to be discussed in section 3.4.

**3.3. Effect of HAuCl<sub>4</sub> Concentration.** When the concentration of HAuCl<sub>4</sub> is decreased from 0.03 to 0.015 M, some changes are also noticed. It can be expected that less HAuCl<sub>4</sub> will have little influence on a 45% polymer system without CTAB or TBAB except for the smaller particle size, as confirmed by comparing TEM images (Figure 7a) and the absorption spectrum (Figure 8a) with those of 0.03 M HAuCl<sub>4</sub> system. But it can be seen from morphologies (parts b–e of Figure 7) that both nanoplates and nanoparticles exist in products. And their corresponding absorption spectra in Figure 8 show that the products tend to be of smaller sizes, present morphological diversity, aggregate more easily, and interact strongly with each other.<sup>19,23,29,30</sup> Such changes are similar to those observed when increasing CTAB or TBAB concentration because of the same tendency by decreasing HAuCl<sub>4</sub> amount.

**3.4. Growth Mechanism of Gold Nano- and Microplates.** From analysis of SAXS and TEM results, it should be noted that the products do not replicate the long-range ordered structure of the hexagonal phase; that is, there is no obviously templating effect occurred in the reaction systems. Evidently, addition of capping agents leads to appearance of microplates. Our results seem to confirm the conclusion from Pileni, i.e., anisotropic nanocrystal formation is more related to selective adsorption of ions during the crystal growth than to the nature of the soft templates.<sup>32</sup> Scheme 1 illustrates a possible mechanism for gold nanocrystal growth, which comprises mainly two

**SCHEME 1: Schematic Growth Mechanism of Gold Microplates from the P123 (45%)–CTAB (1.0%)–HAuCl<sub>4</sub> (0.03 M) System: (a) Cross Section of the Hexagonal Phase, (b) Side View of Two Adjacent Cylinders, and (c) Growth Process of Products**



processes: (i) the formation of Au atoms and/or small clusters in the LLC aqueous domain as the nascent crystal nuclei (I in Scheme 1); (ii) the subsequent anisotropic growth from these nuclei (II and III in Scheme 1).

At the initial stage, the dominant process is metal Au nucleation. During preparation, when light-yellow HAuCl<sub>4</sub> aqueous solution is added to samples containing CTAB, the color is turned to salmon pink within a few minutes, indicating the CTA<sup>+</sup>–AuCl<sub>4</sub><sup>–</sup> complex formation.<sup>6,33</sup> With time going, reduction of Au<sup>III</sup> occurs and the color deepens accompanying small gold nuclei production, which can be verified by absorption spectra in Figure 4A. Noted that, at this period, there are possibly three main factors influencing the nucleation, including LLC structure, CTAB adsorption, and CTA<sup>+</sup>–AuCl<sub>4</sub><sup>–</sup> complex formation. The LLC structure directs gold nuclei being distributed in water domains separated by hydrophobic cylinders, indicating a long-range ordered nuclei arrangement. As for CTAB adsorption, it has been reported in the literature<sup>6,13</sup> to control the gold nanorod production in a bilayer fashion. In our case, CTAB molecules cannot move as freely as in the solution phase because their alkyl chains are interdigitated in the hydrophobic PPO cores inside the cylinders of LLC. Thus the gold nuclei adsorbed by CTAB have to be arranged side by side near the hydrophobic/hydrophilic interface (see Scheme 1). The surfactant–AuCl<sub>4</sub><sup>–</sup> complex, however, retards the nucleation rate, which may thus favor the consequent single crystal growth.<sup>34</sup>

During crystal growth, oriented attachment is considered to be a probable mechanism which gives rise to homogeneous single crystals,<sup>35</sup> though there are some other possibilities for gold plate formation. It involves spontaneous self-organization of adjacent particles so that they share a common crystallographic orientation, followed by joining of these particles at a planar interface.<sup>24,35</sup> On the basis of this mechanism, with more AuCl<sub>4</sub><sup>–</sup> being reduced, nuclei fixed by CTAB molecules orientationally attach and coalesce with adjacent ones, decreasing their surface energy and enhancing platelike nanocrystal production. During this process, CTAB also seems to play the crucial role. We have seen that large microplates can be obtained when CTAB concentration is added to a certain value (1.0% in this system). Exceeding it, more CTAB molecules will reduce the products' size and make them irregular. It has been suggested that atoms on different crystallographic facets might have different interaction strengths with a polymeric or surfactant capping agent, leading to the anisotropic growth of a solid material.<sup>7a,36</sup> In this case, the

binding<sup>6–8,13,32</sup> between CTAB and Au, combining both Br<sup>–</sup> and CTA<sup>+</sup> adsorption, inhibits particles growth randomly and favors flat single-crystal growth with {111} facets extending. It should be noted here that P123, as a poor stabilizer for noble metal,<sup>34</sup> may also play some role of a capping agent, which can be confirmed from the appearance of few Au plates in the P123–HAuCl<sub>4</sub> system. But it is not the key factor in CTAB-containing systems. With CTAB concentration increasing from 0.5 to 1.0%, such capping adsorption induces higher nanocrystal surface coverage and favors a large-scale production of microplates. With plates growing larger, the hexagonal arrays are deformed, inducing decayed SAXS intensities as exhibited in curves a<sub>2</sub>, b<sub>2</sub> and c<sub>2</sub> of Figure 1.

As for smaller nanoparticles produced when CTAB concentration increases, it can be explained by enhanced adsorption of cations and halide ions on gold surfaces.<sup>37</sup> Adding more CTAB (> 1.0%) will lead to more binding of cations and anions with Au and thus an increased mobility of gold surface atoms.<sup>37,38</sup> This effect not only prevents crystals from growing along only certain directions but also makes it easy for unstable small gold nanoparticles to dissolve, aggregate, or fuse to metal clusters.<sup>37,38</sup> Such a process can be testified by parts d and e of Figure 2. It is also consistent with results reported in other systems<sup>5d,37d</sup> and can be used to explain the effect of decreased HAuCl<sub>4</sub> concentration on products.

By comparison to CTAB-added systems, TBAB molecules tend to result in diverse product morphologies. This may be attributed to its short less-hydrophobic butyl groups, which makes it act more like a cosurfactant and be located at the polar/apolar interface in LLC but not interdigitated into PPO domains. Therefore TBAB could move more freely than CTAB, accompanying a less oriented attachment of gold nuclei. Such effects may enhance the gold aggregation in a different direction, resulting in product morphological diversity.<sup>35a,37c</sup>

#### 4. Conclusions

In summary, we have established a novel and simple method for controllable preparation of gold nano- and microplates. During plate growth, added CTAB or TBAB molecules may play the crucial role in controlling the shape and size by adsorbing selectively on certain crystallographic facets. We find there is an optimal value of capping agent concentration for obtaining gold microplates. In excess of this value, diverse morphologies would be formed because CTAB or TBAB headgroups and Br<sup>–</sup> can bind with Au in different direction besides {111} facets. Although the morphology of gold products does not replicate the long-range ordered structure of hexagonal phase, the templating effect indeed occurs at the first stage on CTAB and gold nuclei arrangement, which is important for flat product formation. Therefore the LLC phase provides an ideal reaction environment to control the shape of gold particles. Obtained results suggest an effective way to produce particles with controllable shape and size as well as a clue to understand the mechanism for crystal growth.

**Acknowledgment.** We thank the supports from the National Natural Science Foundation of China (20073025, 20373035), Specialized Research Fund for the Doctoral Program of Higher Education (20020422060), and Excellent Young Scientists Awarding Found of Shandong Province (01BS21).

#### References and Notes

- (1) (a) Wang, Z. L. *Adv. Mater.* **1998**, *10*, 13. (b) Shipway, A. N.; Katz, E.; Willner, I. *ChemPhysChem* **2000**, *1*, 18. (c) Cui, Y.; Lieber, C.

- M. *Science* **2001**, 291, 851. (d) Maier, S. A.; Brongersma, M. L.; Kik, P. G.; Meltzer, S.; Requicha, A. A. G.; Atwater, H. A. *Adv. Mater.* **2001**, 13, 1501. (e) Nicewarner-Pena, S. R.; Freeman, R. G.; Reiss, B. D.; He, L.; Pena, D. J.; Walton, I. D.; Cromer, R.; Keating, C. D.; Natan, M. J. *Science* **2001**, 294, 137. (f) Lee, S.-M.; Cho, S.-N.; Cheon, J. *Adv. Mater.* **2003**, 15, 441. (g) Daniel, M.-C.; Astruc, D. *Chem. Rev.* **2004**, 104, 293.
- (2) (a) Markovich, G.; Collier, C. P.; Henrichs, S.; Remacle, F. O.; Levine, R. D.; Heath, J. R. *Acc. Chem. Res.* **1999**, 32, 415. (b) Link, S.; El-Sayed, M. A. *Int. Rev. Phys. Chem.* **2000**, 19, 409. (c) Coronado, E. A.; Schatz, G. C. *J. Chem. Phys.* **2003**, 119, 3926.
- (3) (a) Hu, J.; Odom, T. W.; Lieber, C. M. *Acc. Chem. Res.* **1999**, 32, 435. (b) Jun, Y.; Lee, S.-M.; Kang, N.-J.; Cheon, J. *J. Am. Chem. Soc.* **2001**, 123, 5150. (c) Sun, Y.; Xia, Y. *Science* **2002**, 298, 2176. (d) Sun, Y.; Mayers, B.; Xia, Y. *Nano Lett.* **2003**, 3, 675. (e) Chen, S.; Wang, Z. L.; Ballato, J.; Foulger, S. H.; Carroll, D. L. *J. Am. Chem. Soc.* **2003**, 125, 16186. (f) Wang, W.; Bai, F. *ChemPhysChem* **2003**, 4, 761. (g) Zhang, D.; Qi, L.; Yang, J.; Ma, J.; Cheng, H.; Huang, L. *Chem. Mater.* **2004**, 16, 872.
- (4) Haynes, C. L.; Van Duyne, R. P. *J. Phys. Chem. B* **2001**, 105, 5599.
- (5) (a) Murphy, C. J.; Jana, N. R. *Adv. Mater.* **2002**, 14, 80. (b) Jana, N. R.; Gearheart, L.; Murphy, C. J. *J. Phys. Chem. B* **2001**, 105, 4065. (c) Sau, T. K.; Murphy, C. J. *Langmuir* **2004**, 20, 6414. (d) Johnson, C. J.; Dujardin, E.; Davis, S. A.; Murphy, C. J.; Mann, S. *J. Mater. Chem.* **2002**, 12, 1765. (e) Gole, A.; Murphy, C. J. *Chem. Mater.* **2004**, 16, 3633.
- (6) Gao, J.; Bender, C. M.; Murphy, C. J. *Langmuir* **2003**, 19, 9065.
- (7) (a) Sun, Y.; Mayers, B.; Herricks, T.; Xia, Y. *Nano Lett.* **2003**, 3, 955. (b) Yu, Y.-Y.; Chang, S. S.; Lee, C.-L.; Wang, C. R. C. *J. Phys. Chem. B* **1997**, 101, 6661. (c) Link, S.; Mohamed, M. B.; El-Sayed, M. A. *J. Phys. Chem. B* **1999**, 103, 3073. (d) Kim, F.; Song, J.; Yang, P. *J. Am. Chem. Soc.* **2002**, 124, 14316.
- (8) Aguirre, C. M.; Kaspar, T. R.; Radloff, C.; Halas, N. J. *Nano Lett.* **2003**, 3, 1707.
- (9) Nikoobakht, B.; Wang, Z. L.; El-Sayed, M. A. *J. Phys. Chem. B* **2000**, 104, 8635.
- (10) (a) Busbee, B. D.; Obare, S. O.; Murphy, C. J. *Adv. Mater.* **2003**, 15, 414. (b) Zhu, Y.-J.; Hu, X.-L. *Chem. Lett.* **2003**, 32, 1140.
- (11) (a) Jana, N. R.; Gearheart, L.; Murphy, C. J. *Chem. Commun.* **2001**, 617. (b) Brown, K. R.; Walter, D. G.; Natan, M. J. *Chem. Mater.* **2000**, 12, 306.
- (12) (a) El-Sayed, M. A. *Acc. Chem. Res.* **2001**, 34, 257. (b) Mohamed, M. B.; Volkov, V.; Link, S.; El-Sayed, M. A. *Chem. Phys. Lett.* **2000**, 317, 517. (c) El-Sayed, M. A.; Nikoobakht, B. *Chem. Mater.* **2003**, 15, 1957.
- (13) Nikoobakht, B.; El-Sayed, M. A. *Langmuir* **2001**, 17, 6368.
- (14) (a) Chen, S.; Carroll, D. L. *Nano Lett.* **2002**, 2, 1003. (b) Pastoriza-Santos, I.; Liz-Marzan, L. M. *Nano Lett.* **2002**, 2, 903. (c) Hao, E.; Kelly, K. L.; Hupp, J. T.; Schatz, G. C. *J. Am. Chem. Soc.* **2002**, 124, 15182. (d) Jin, R.; Cao, Y. W.; Mirkin, C. A.; Kelly, K. L.; Schatz, G. C.; Zheng, J. G. *Science* **2001**, 294, 1901. (e) Jiang, L.-P.; Xu, S.; Zhu, J.-M.; Zhang, J.-R.; Zhu, J.-J.; Chen, H.-Y. *Inorg. Chem.* **2004**, 43, 5877. (f) Chen, S.; Carroll, D. L. *J. Phys. Chem. B* **2004**, 108, 5500.
- (15) (a) Maillard, M.; Giorgio, S.; Pileni, M.-P. *J. Phys. Chem. B* **2003**, 107, 2466. (b) Maillard, M.; Huang, P.; Brus, L. *Nano Lett.* **2003**, 3, 1611. (c) Maillard, M.; Giorgio, S.; Pileni, M.-P. *Adv. Mater.* **2002**, 14, 1084. (d) Chen, S.; Fan, Z.; Carroll, D. L. *J. Phys. Chem. B* **2002**, 106, 10777. (e) Germain, V.; Li, J.; Ingert, D.; Wang, Z. L.; Pileni, M. P. *J. Phys. Chem. B* **2003**, 107, 8718.
- (16) Mock, J. J.; Barbic, M.; Smith, D. R.; Schultz, D. A.; Schultz, S. *J. Chem. Phys.* **2002**, 116, 6755.
- (17) (a) Milligan, W. O.; Morriss, R. H. *J. Am. Chem. Soc.* **1964**, 86, 3461. (b) Turkevich, J.; Stevenson, P. C.; Hillier, J. *J. Discuss. Faraday Soc.* **1951**, 11, 55.
- (18) Stoeva, S. I.; Prasad, B. L. V.; Uma, S.; Stoimenov, P. K.; Zaikovski, V.; Sorensen, C. M.; Klabunde, K. J. *J. Phys. Chem. B* **2003**, 107, 7441.
- (19) Malikova, N.; Pastoriza-Santos, I.; Schierhorn, M.; Kotov, N. A.; Liz-Marzan, L. M. *Langmuir* **2002**, 18, 3694.
- (20) Zhou, Y.; Wang, C. Y.; Zhu, Y. R.; Chen, Z. Y. *Chem. Mater.* **1999**, 11, 2310.
- (21) Ibano, D.; Yokota, Y.; Tominaga, T. *Chem. Lett.* **2003**, 32, 574.
- (22) Tsuji, M.; Hashimoto, M.; Nishizawa, Y.; Tsuji, T. *Chem. Lett.* **2003**, 32, 1114.
- (23) (a) Shankar, S. S.; Rai, A.; Ankamwar, B.; Singh, A.; Ahmad, A.; Sastry, M. *Nature Mater.* **2004**, 3, 482. (b) Kim, J.-U.; Cha, S.-H.; Shin, K.; Jho, J. Y.; Lee, J.-C. *Adv. Mater.* **2004**, 16, 459. (c) Sun, X.; Dong, S.; Wang, E. *Angew. Chem., Int. Ed.* **2004**, 43, 6360.
- (24) Wang, L.; Chen, X.; Zhan, J.; Sui, Z.; Zhao, J.; Sun, Z. *Chem. Lett.* **2004**, 33, 720.
- (25) Holmqvist, P.; Alexandridis, P.; Lindman, B. *J. Phys. Chem. B* **1998**, 102, 1114.
- (26) Firestone, M. A.; Williams, D. E.; Seifert, S.; Csencsits, R. *Nano Lett.* **2001**, 1, 129.
- (27) (a) Andersson, M.; Alfredsson, V.; Kjellin, P.; Palmqvist, A. E. C. *Nano Lett.* **2002**, 2, 1403. (b) Liz-Marzan, L. M.; Lado-Tourino, I. *Langmuir* **1996**, 12, 3585. (c) Qi, L.; Gao, Y.; Ma, J. *Colloids Surf. A* **1999**, 157, 285.
- (28) Pinna, N.; Weiss, K.; Urban, J.; Pileni, M.-P. *Adv. Mater.* **2001**, 13, 261.
- (29) (a) Jiang, C.; Markutsya, S.; Tsukruk, V. V. *Langmuir* **2004**, 20, 882. (b) Gupta, R.; Dyer, M. J.; Weimer, W. A. *J. Appl. Phys.* **2002**, 92, 5264. (c) Mayya, K. S.; Patil, V.; Sastry, M. *Bull. Chem. Soc. Jpn.* **2000**, 73, 1757. (d) Cheng, W.; Dong, S.; Wang, E. *Angew. Chem.* **2003**, 115, 465. (e) Shipway, A. N.; Lahav, M.; Gabai, R.; Willner, I. *Langmuir* **2000**, 16, 8789.
- (30) (a) Wang, W.; Efrima, S.; Regev, O. *J. Phys. Chem. B* **1999**, 103, 5613. (b) Chen, C.-D.; Yeh, Y.-T.; Wang, C. R. C. *J. Phys. Chem. Solids* **2001**, 62, 1587. (c) Westcott, S. L.; Oldenburg, S. J.; Lee, T. R.; Halas, N. J. *Chem. Phys. Lett.* **1999**, 300, 651. (d) Kim, B.; Tripp, S. L.; Wei, A. J. *Am. Chem. Soc.* **2001**, 123, 7955. (e) Pei, L. H.; Mori, K.; Adachi, M. *Langmuir* **2004**, 20, 7837.
- (31) (a) Kamat, P. V.; Flumiani, M.; Hartland, G. V. *J. Phys. Chem. B* **1998**, 102, 3123. (b) Kreibitz, U.; Vollmer, M. *Optical Properties of Metal Cluster*; Springer: Berlin, 1995.
- (32) (a) Pileni, M.-P. *Nature Mater.* **2003**, 2, 145. (b) Filankembo, A.; Giorgio, S.; Lisiecki, I.; Pileni, M. P. *J. Phys. Chem. B* **2003**, 107, 7492.
- (33) (a) Kameo, A.; Suzuki, A.; Torigoe, K.; Esumi, K. *J. Colloid Interface Sci.* **2001**, 241, 289. (b) Torigoe, K.; Esumi, K. *Langmuir* **1992**, 8, 59.
- (34) Mayer, A.; Antonietti, M. *Colloid Polym. Sci.* **1998**, 276, 769.
- (35) (a) Alivisatos, A. P. *Science* **2000**, 289, 736. (b) Penn, R. L.; Banfield, J. F. *Science* **1998**, 281, 969. (c) Penn, R. L.; Oskam, G.; Strathmann, T. J.; Searson, P. C.; Stone, A. T.; Veblen, D. R. *J. Phys. Chem. B* **2001**, 105, 2177. (d) Banfield, J. F.; Welch, S. A.; Zhang, H.; Ebert, T. T.; Penn, R. L. *Science* **2000**, 289, 751.
- (36) Brown, S.; Sarikaya, M.; Johnson, E. *J. Mol. Biol.* **2000**, 299, 725.
- (37) (a) Zou, S.; Gao, X.; Weaver, M. J. *Surf. Sci.* **2000**, 452, 44. (b) Paik, W.; Genshaw, M. A.; Bockris, J. O. *J. Phys. Chem.* **1970**, 74, 4266. (c) Yonezawa, T.; Onoue, S.; Kimizuka, N. *Chem. Lett.* **2002**, 31, 1172. (d) Ishizuka, H.; Tano, T.; Torigoe, K.; Esumi, K.; Meguro, K. *Colloids Surf.* **1992**, 63, 337.
- (38) Li, G.; Lauer, M.; Schulz, A.; Boettcher, C.; Li, F.; Fuhrhop, J.-H. *Langmuir* **2003**, 19, 6483.